Proceedings of FEDSM'03:
4th ASME/JSME Joint Fluids Engineering Conference
Honolulu, Hawaii, USA, July 6-10, 2003

FEDSM2003-45535

HYDRODYNAMIC MODEL FOR MICROSCALE FLOWS IN A CHANNEL WITH TWO 90^O BENDS

Reni Raju and Subrata Roy
Computational Plasma Dynamics Laboratory
Department of Mechanical Engineering
Kettering University
Flint, MI 48504, USA
E-mail: sroy@kettering.edu

ABSTRACT

Many microfluidic devices require serpentine channels to allow longer contact length within a compact area. The necessity of understanding the physical laws governing these complicated small geometries is crucial for better design of practical microfluidic systems. At micro-scales the continuum assumption of standard Navier-Stokes equation is no longer valid as the mean free path of the fluid becomes comparable to the dimension of the system. A finite element based hydrodynamic algorithm has been developed recently for analyzing slip flows through two-dimensional micro geometries. This paper documents numerical results for gas flow through a micro-column with two sharp 90° bends. The results obtained show increase in slip effect for higher pressure ratios. To the best of our knowledge, this is the first such published report addressing microflow in this particular geometry.

INTRODUCTION

Over the past decade micromachinining technology has shown rapid development enabling manufacturing of complex microelectromechanical systems (MEMS). Microscale pumps, turbines, thrusters, sensors and actuators are a few examples of these small-scale devices. The reduction in scale increases the complexity of these systems. Physical laws governing these devices vary greatly from macro scale systems, especially from the fluidics perspective.

Experiments suggest that the standard Navier-stokes equations cannot predict the flow through these devices accurately. At these scales the fluid behavior tends to become rarefied (molecular) and the walls "move" as the mean free path of the gas becomes comparable to the length scale of the system. The continuum model no longer can predict the flow without accommodating other factors like rarefaction, compressibility, viscous dissipation and thermal creep effects [1] at these scales for gaseous flows. The Knudsen number is a measure of the degree of rarefaction of gases encountered in small flows through narrow channels. It is defined as the ratio of the fluid mean free path, λ and the macroscopic length scale of the physical system, Λ.

$$\mathrm{Kn} = \frac{\lambda}{\Lambda} \qquad (1)$$

In Eq. (1), $\lambda = 16\mu \Big/ \left(5\rho\sqrt{2\pi RT}\right)$, using the Chapman-Enskog relation for the coefficient of dynamic viscosity μ in a hard sphere gas at temperature T, and $\Lambda = \rho/(\partial\rho/\partial x)$. As $\mathrm{Kn} \to 0$ the flow can be assumed sufficiently continuous while for $\mathrm{Kn} > 10$ it becomes a free-molecule flow [2]. However for $0.001 < \mathrm{Kn} < 10$ the flow is neither sufficiently continuum nor completely molecular, hence has been further divided into two subcategories; slip-flow regime for $0.001 < \mathrm{Kn} < 0.1$ and transition regime for $0.1 < \mathrm{Kn} < 10$.

Researchers have applied various numerical techniques for validating the computational models with the experimental data in slip and transition regimes of low speed flows. Harley *et al.* [3] has used a two-dimensional finite element technique for evaluating the compressible flow between two parallel plates, however without considering the slip effects. Liu *et al.* [4, 5] have conducted both experiments and modeling of pressure distribution in microchannels. Chen *et al*. [6] have studied the experimental results of Pong *et al*. [7] and Arkilic *et al.* [8] using the finite difference method with slip boundary conditions. Arkilic *et al*. [8, 9] have done two-dimensional analysis of Navier-Stokes equation with first-order slip boundary conditions to study compressibility and rarefied effects in long microchannels. Beskok and Karniadakis [10, 11] have carried out both analytical and numerical study of flow in several micro geometries using direct simulation Monte Carlo (DSMC) and spectral element method [10]. Available DSMC, molecular dynamics and Burnett equation methods and their limitations are listed elsewhere [12].

This paper aims to apply a computationally efficient hydrodynamic algorithm developed at CPDL by Roy *et al.* [12] for complex micro-geometries. Present study focuses on flow through a micro-column with two sharp 90° bends, which is a geometric modification of the straight microchannel studied by Poiseuille flow [6,7]. The subject geometry has applications in many practical microfluidic devices that require serpentine channels to allow longer contact length within a compact area. Following sections cover the model description, governing hydrodynamic equations, finite element algorithm and discussion of numerical results. The solution obtained for the bends are also compared to the reported numerical results for the straight microchannel [12]. To the best of our knowledge, no other published report has addressed microflow in this particular geometry.

NOMENCLATURE

C_p	Specific heat at constant pressure
H	Height of the micro-column
Kn	Knudsen number
L	Centerline length of the micro-column
N	Basis function
P	Gas pressure
Pr	Prandtl number
R	Specific gas constant
$\mathbb{R}$	Real Space
T	Gas temperature
W	Width of the micro-column
d	Problem dimension
t	Time
u	Velocity in the x-direction
v	Velocity in the y-direction
x	Cartesian direction
y	Cartesian direction

Greek

$\in$	Convergence criteria
ε	Diffusion coefficient
γ	Ratio of specific heats
κ	Thermal conductivity
λ	Mean free path of the gas
Λ	Characteristic dimension
μ	Absolute viscosity
Ω	Solution domain
ρ	Gas density
σ_V	Tangential momentum accommodation coefficient
σ_T	Thermal accommodation coefficient
τ	Area

Subscript

e	Finite element
gas	of Gas
k	Degree of basis polynomial
$wall$	at Wall

Superscript

h	Mesh measure

MODEL DESCRIPTION

The two-dimensional micro-column geometry under consideration is shown in Fig. 1. The overall dimensions of the microchannel with two 90° bends are based on the first generation straight microchannel system [7].

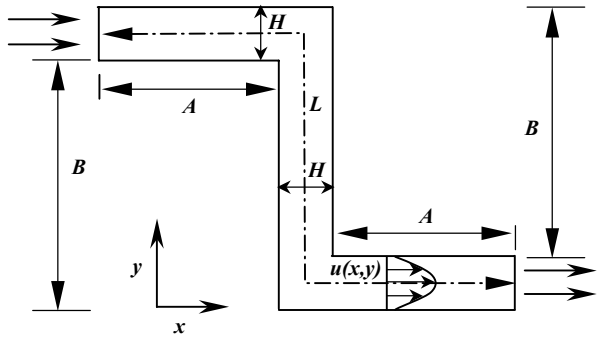

Fig 1: Geometry schematic used for microflow analysis.

The centerline length L, height H and width W remain the same as in Ref. [7]. For two-dimensional analysis the end effects across the width W (normal to the xy-plane) have been ignored. The working fluid is Nitrogen and its properties along with other flow parameters are listed in Table 1. The aspect ratio of the channel is 2500 with a centerline length of 3000 μm and the Knudsen number at the outlet is 0.0585 for the given atmospheric conditions.

Table 1: Model dimensions and gas properties

Parameters	Value
Centerline length, $\boldsymbol{L}$	3000 μm
Length, $\boldsymbol{A}$	999.4 μm
Length, $\boldsymbol{B}$	1000 μm
Width, $\boldsymbol{W}$	40 μm
Height, $\boldsymbol{H}$	1.2 μm
Pressure Ratio, $\boldsymbol{P_{in}/P_{out}}$	1.34, 1.68, 2.02, 2.36, 2.70
Outlet Pressure, $\boldsymbol{P_{out}}$	100.8 kPa
Temperature at the Inlet, $\boldsymbol{T_i}$	314 K
Wall Temperature, $\boldsymbol{T_w}$	314 K
Exit Knudsen Number, **Kn**	0.0585
Absolute viscosity, $\boldsymbol{\mu}$	1.85×10^{-5} Ns/m^2
Specific gas constant, $\boldsymbol{R}$	296.8 J/kg K
Ratio of specific heats, $\boldsymbol{\gamma}$	1.4

GOVERNING EQUATIONS

The following two-dimensional Navier Stokes equations with constant viscosity govern the system.

Conservation of mass:

$$\frac{\partial \rho}{\partial t} + \frac{\partial \rho u}{\partial x} + \frac{\partial \rho v}{\partial y} = 0 \qquad (2)$$

Conservation of x- momentum:

$$\frac{\partial \rho u}{\partial t}+u\frac{\partial \rho u}{\partial x}+v\frac{\partial \rho u}{\partial y}+\frac{\partial P}{\partial x}-\mu\left(\frac{\partial^2 u}{\partial x^2}+\frac{\partial^2 u}{\partial y^2}+\frac{1}{3}\left(\frac{\partial^2 u}{\partial x^2}+\frac{\partial^2 v}{\partial x \partial y}\right)\right)=0 \qquad (3)$$

Conservation of y- momentum:

$$\frac{\partial \rho v}{\partial t}+u\frac{\partial \rho v}{\partial x}+v\frac{\partial \rho v}{\partial y}+\frac{\partial P}{\partial y}-\mu\left(\frac{\partial^2 v}{\partial x^2}+\frac{\partial^2 v}{\partial y^2}+\frac{1}{3}\left(\frac{\partial^2 v}{\partial y^2}+\frac{\partial^2 u}{\partial x \partial y}\right)\right)=0 \qquad (4)$$

Conservation of energy:

$$\begin{aligned}&\rho Cp\frac{DT}{Dt}-\frac{DP}{Dt}-\frac{\partial}{\partial x}\left(\kappa\frac{\partial T}{\partial x}\right)-\frac{\partial}{\partial y}\left(\kappa\frac{\partial T}{\partial y}\right)\\&-\mu\left(2\left(\frac{\partial u}{\partial x}\right)^2+2\left(\frac{\partial v}{\partial y}\right)^2+\left(\frac{\partial v}{\partial x}+\frac{\partial u}{\partial y}\right)^2-\frac{2}{3}\left(\frac{\partial u}{\partial x}+\frac{\partial v}{\partial y}\right)^2\right)=0\end{aligned} \qquad (5)$$

The equation of state is defined using the ideal gas law,

$$P - \rho RT=0 \qquad (6)$$

For the 'no-slip' wall condition in continuum description, all components of the velocity vanish at the solid wall. As the system length scale becomes comparable to the mean free path of the working fluid, the streaming velocity at the wall becomes important and can be described comprising of the streaming velocity of incident particles and that of the scattered particles. The boundary condition in this case can be interpreted as the flux or Neumann condition from the macroscopic point of view. One may, of course, use a Taylor series expansion on mean free path (Knudsen number) to determine the wall streaming velocity as a function of normal derivatives. Maxwell [13] derived the first order slip relations for dilute, monatomic gases. We shall implement first order slip boundary conditions in the momentum and energy equations for $10^{-3}< \mathrm{Kn} <10^{-1}$.The wall-slip boundary condition for an ideal gas is given as,

$$u_{gas}-u_{wall}=\frac{2-\sigma_V}{\sigma_V}\lambda\left(\frac{\partial u}{\partial y}\right)_{wall}+\frac{3}{4}\frac{\mu}{\rho T_{gas}}\left(\frac{\partial T}{\partial x}\right)_{wall} \qquad (7a)$$

The corresponding temperature-jump relation was derived by von Smoluchowski [14] as,

$$T_{gas}-T_{wall}=\frac{2-\sigma_T}{\sigma_T}\left[\frac{2\gamma}{\gamma+1}\right]\frac{\lambda}{\mathrm{Pr}}\left(\frac{\partial T}{\partial y}\right)_{wall} \qquad (7b)$$

The slip-wall conditions (7a)-(7b) use the tangential-momentum accommodation coefficient, σ_v and the thermal accommodation coefficient, σ_T at the walls. These coefficients indicate the fraction of the molecules reflected diffusively from the walls. For example, molecules reflect *specularly* for $\sigma_v = 0$ indicating the reversal in their normal velocity due to normal momentum transfer to the wall. For $\sigma_v = 1$ the molecules reflect *diffusively* when reflected from the wall with zero average tangential velocity. The value of the coefficients σ_V and σ_T depends on the different parameters like the surface finish, the fluid, temperature and local pressure. The value of σ_V ranging from 0.75-0.85 for nitrogen, argon or carbon dioxide in a silicon micromachined channel have been determined experimentally by Arkilic [16, 17].

Equations (7a-7b) are applicable as long as Kn < 0.1, for Kn higher than that it maybe difficult to obtain accurate solution with just the first order slip boundary conditions. Beskok and Karniadakis [17] have presented a second-order accurate slip boundary condition for predicting higher Knudsen number flows. Studies by Sreekanth [18] and Piekos and Breuer [19] suggest Maxwell's first order boundary condition breaks down near Kn = 0.15. However contrary to the common practice, Roy *et al*. [12] have used the first-order boundary condition for higher Knudsen number (7.36). The present problem has an outlet Knudsen number of 0.0585.

NUMERICAL PROCEDURE

Algorithms developed using finite element method are extensively used in numerical simulation of heat transfer and fluid flow [20,21]. Recently, Roy and Pandey have implemented it for analyzing the partially ionized gas flow inside an electric propulsion device [22,23]. Roy *et al.* [12] have utilized the finite element formulation [22-25] to predict the gaseous flow through the micro- and nano-geometries by implementation of the first-order slip boundary condition.

The equation system (2)-(6) can be written in the conservative form for any state variable, e.g., $u = u(x_j)$ in the form,

$$L(u) \equiv 0 \qquad (8)$$

Note that u in Eq. (8) can be density, velocity components, temperature, kinetic energy and dissipation.

The integral associated with the *weak statement* [25] for Eq. (8) is

$$\int_\Omega wL(u)\,d\Omega = 0 \qquad (9)$$

where w is any admissible test function [26]. Thereafter the FE spatial semi-discretization of the domain Ω of Eq. (8) employs the mesh $\Omega^h = \bigcup_e \Omega_e$, and Ω_e is the generic computational domain. Using the superscript h to denote the 'spatial discretization', the FE weak statement implementation for Eqs. (8) and (9) defines the approximation as,

$$u(x_j) \approx u^h(x_j) = \bigcup_e u_e(x_j)\,, \qquad (10)$$

$$u_e(x_j) = \{N_k\}^{\mathrm{T}}\{\mathrm{U}\}_e\,, \qquad (11)$$

where {.} denotes a column matrix, and the trail space FE basis set $\{N_k(x_j)\}$ typically contains Chebyshev, Lagrange or Hermite interpolation polynomials complete to the degree k.

The spatially semi-discrete FE implementation of the *weak statement* WS^h for Eq. (9) leads to

$$WS^h = S_e \left(\int_{\Omega_e} N_k L_e(\mathbf{U}) d\tau \right) \tag{12}$$

S_e symbolizes the "assembly operator" carrying local (element) matrix coefficients into the global arrays. Application of Green-Gauss divergence theorem in Eq. (12) will yield natural homogenous Neumann boundary conditions. The advantage of using finite element method is that the weak statement yields the surface integral in Eq. (12) which contains the unknown boundary fluxes wherever Dirichlet (fixed) boundary conditions are enforced. For the slip flow regime the boundary fluxes are replaced by incorporating the weak statements of Eq. (7a-7b) into surface integral function of the momentum and energy equations.

Independent of the physical dimension of Ω, and for general forms of the flux vectors, the semi-discretized weak statement of Eq. (12) always yields an ordinary differential equation (ODE) system:

$$\mathbf{M} \frac{d\mathbf{U}}{d\mathbf{t}} + \mathbf{R}(\mathbf{U}) = 0, \tag{13}$$

where $\mathbf{U}(t)$ is the time-dependent finite element nodal vector. The time derivative $d\mathbf{U}/dt$, is generally replaced with a ϑ-implicit or τ-step Runge-Kutta time integration procedure. In Eq. (13), $\mathbf{M} = S_e(\mathbf{M}_e)$ is the "mass" matrix associated with element level interpolation, $\mathbf{R}$ carries the element convection information and the diffusion matrix resulting from genuine (non-Eulerean) or numerical elemental viscosity effects, and all known data. Equation (13) is usually solved using a Newton-Raphson scheme,

$$\mathbf{U}_{\tau+1}^{i+1} = \mathbf{U}_{\tau+1}^{i} + \Delta\mathbf{U}^{i} = \mathbf{U}_{\tau} + \sum_{p=0}^{i} \mathbf{U}^{p+1},$$
$$\text{where } \Delta\mathbf{U}^{i} = -\left[\mathbf{M} + \vartheta\Delta t(\partial\mathbf{R}/\partial\mathbf{U})\right]^{-1} \mathbf{R}(\mathbf{U}) \tag{14}$$

In Eq. (14), ϑ is the implicitness of the numerical algorithm and $0 < \vartheta < 1$. The obvious numerical issues will be associated with calculation of the "jacobian", $\partial\mathbf{R}/\partial\mathbf{U}$, and inversion of the $\mathbf{M}+\vartheta\Delta t(\partial\mathbf{R}/\partial\mathbf{U})$ matrix with sufficient accuracy.

The algorithm is solved using fully implicit variable time steps until the transient features die down as the Newton-Raphson iteration converges to a steady state. The choice of time step is dictated by the Courant-Fredrich-Levy condition [27]. The solution is declared convergent when the maximum residual for each of the state variables becomes smaller than a chosen convergence criterion of $\in=10^{-4}$. Here, the convergence of a solution vector $\mathbf{U}$ on node j is defined as the norm: $\|\mathbf{U}_j - \mathbf{U}_{j-1}\| / \|\mathbf{U}_j\| \leq \in$.

The computational column geometry is discretized using two-dimensional 9-noded biquadratic finite elements. The continuity and equation of state are solved for pressure and density respectively using the four corner nodes of the element. For velocity and temperature calculations, all nine nodes of the biquadratic element are used.

BOUNDARY CONDITIONS

The gas temperature T_i at the inlet is specified as 314 K. A uniform wall temperature T_w is also specified as 314 K. The velocity flux $\partial u/\partial x=0$ and the y-component of the velocity $v = 0$ is specified at the inlet. The micro-column is benchmarked using both no-slip and first order slip conditions. For no-slip conditions $u=0$ and $v=0$ is used on the walls, while Eqns. (7a-7b) are used for the slip boundary conditions. For slip boundary since the roughness of the channel is not known, we assume $\sigma_V = \sigma_T \approx 1.0$, implying that the channel surface is rough. This is applicable to most of the engineering systems [15]. The pressure at the outlet, P_0 is maintained at 100.8 kPa while the inlet pressure, P_i is specified based on the pressure ratio.

RESULTS AND DISCUSSIONS

The flow through the channel has been analyzed for both slip and no-slip boundary conditions. The computational domain is discretized using 560 (28 along L, 20 along H in Fig. 1) two-dimensional biquadratic finite elements that consist of 2337 nodes. For a 90° bend the flow undergoes skewing due to the change in streamwise direction in comparison to the flow through a straight duct. In Fig. 2(a), the no-slip condition the flow shows a skewed parabolic profile with a zero velocity on the walls, while for the slip boundary condition there is an increase in the curvature showing relatively higher velocities at the walls and the center, Fig. 2(b).

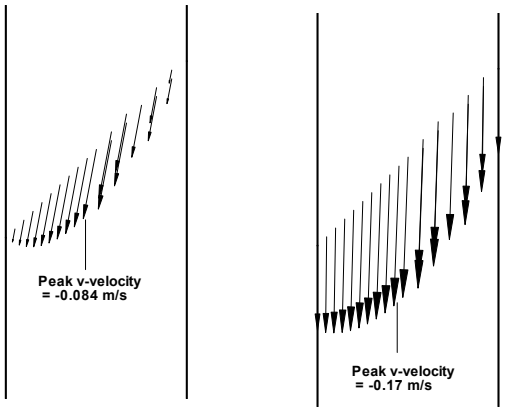

(a) No-slip (b) Slip

Fig 2: Downstream velocity vectors in the micro-column for P_{in}/P_{out}=2.701. The peak v-velocities are shown at the centerline distance of 1200 μm from the inlet.

For this geometry and boundary specifications, the pressure, density and velocity vary non-linearly along the microchannel. The difference in temperature over the computational domain is negligible resulting in almost isothermal condition. The pressure drop occurs to overcome the frictional forces along the channel. For a simple Poiseuille flow the velocity increases downstream to preserve the continuity equation. The rise in shear stress due to the increase in velocity causes a further drop in pressure. The centerline effect shows a relatively higher slope in pressure drop when the flow becomes vertical, Fig. 3.

This is due to the higher shear stress caused by the sharp change in momentum at the bends. Increasing pressure ratios show increasing divergence in the pressure distribution between the no-slip and slip wall solutions. For five selected pressure ratios, the no-slip solutions show a steeper slope in the vertical section than in slip solutions, Fig. 3. This effect is the most prominent for pressure ratio P_{in}/P_{out} = 2.701 where the difference in the pressure distribution between the two predictions is ~-6% at the first bend and ~+10% at the downstream bend.

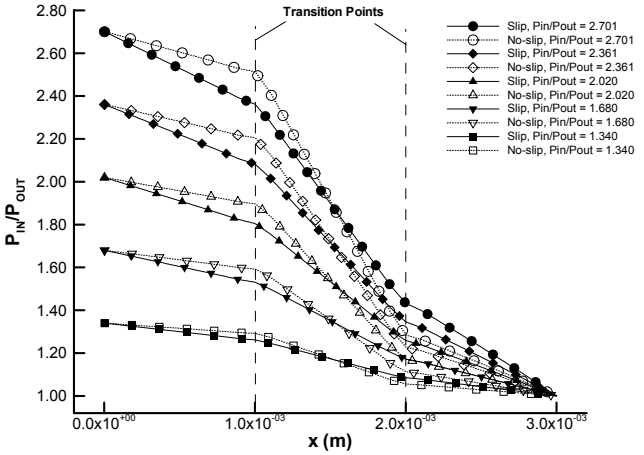

Fig 3: Pressure distribution comparison of slip and no-slip boundary condition along the centerline of the micro-column with 90° bend.

Pong *et al.* [7] have carried out experimental measurements for pressure distribution along a straight microchannel using four pressure sensors along the length of the channel. This first generation microchannel was used to validate the numerical results obtained for same geometry earlier [12]. A comparison of the numerical slip results of the straight and 90° bend shows a marked difference in the pressure distribution, Fig. 4. The

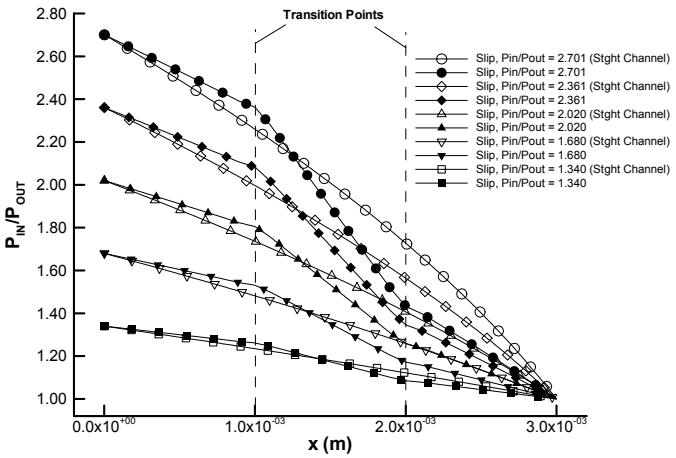

Fig 4: Pressure distribution comparison of numerical results for the micro-column with 90° bend and a straight microchannel [7] with slip flow along the centerline.

change in direction of flow at the bends causes a change in slope at these transition points. The pressure drop in the three sections however tends to be more linear than for a straight channel. For five selected pressure ratios, the distribution for the bend show a maximum difference of ~+4% at the upstream bend and ~-20% along the downstream bend. The difference becomes larger as the pressure ratio increases.

For a Poiseuille flow the drop in pressure leads to corresponding increase in the axial velocity. For the micro-column the *u*-velocity increases till the first transition point and then encounters a sudden drop (to nearly zero) due to change in direction of the flow, Fig. 5. The *u*-velocity again picks up at the second transition point (bend). The increase in velocity is proportionate to the pressure ratio for a fixed outlet pressure. The slip condition indicates that lesser frictional force has to be overcome on the walls, which in turn generates a higher velocity as compared to the no-slip condition. Thus the slip flow shows nearly 55% more velocity at the peak point than no-slip condition for P_{in}/P_{out} =2.701. The small negative values of *u*-velocity at two bends may indicate re-circulation as flow turns sharply.

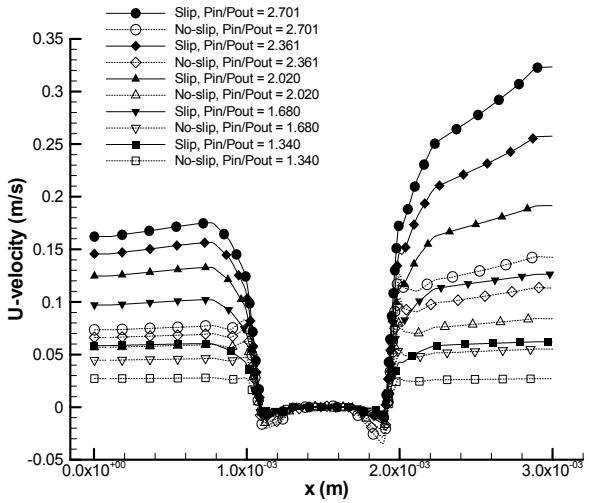

Fig 5: *U* velocity distribution comparison of slip and no-slip boundary condition along the centerline of the micro-column with 90° bends.

Since the primary flow occurs in both *x* and *y* directions along the three sections of the channel, the stream-wise velocity changes from *u* to *v* at the first bend and vice versa at the second. In Fig. 6, as the gas flow turns in the negative *y*-direction, a negative *v* value is seen. The difference in the slip and no-slip values of the *v*-velocity is also plotted in Fig. 6. The centerline distribution shows a sharp rise in the magnitude of velocity in the vertical section, a trend proportionate to rise in *u* in the horizontal sections, and is essentially zero for the rest of the domain. Similar to *u* for higher pressure ratios the difference is higher between slip and no-slip flows. The positive values at transition points may be indicative of the local re-circulation.

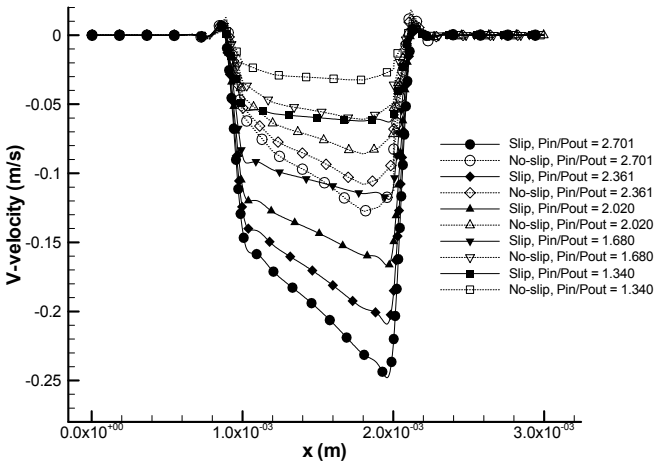

Fig 6: *V*- velocity distribution comparison of slip and no-slip boundary condition along the centerline of the micro-column with 90^o bends.

Fig. 7 compares the massflow rate vs the pressure ratios for slip and no-slip conditions. Upto 2.4 times more massflow rates are observed for slip flows than for the no-slip condition due to lower shear stress on the walls resulting in less momentum exchange. As compared to the straight microchannel the gas flow inside the micro-column with two 90^o bends has to overcome relatively higher shear stress reducing the overall massflow rate by approximately 0.4 times.

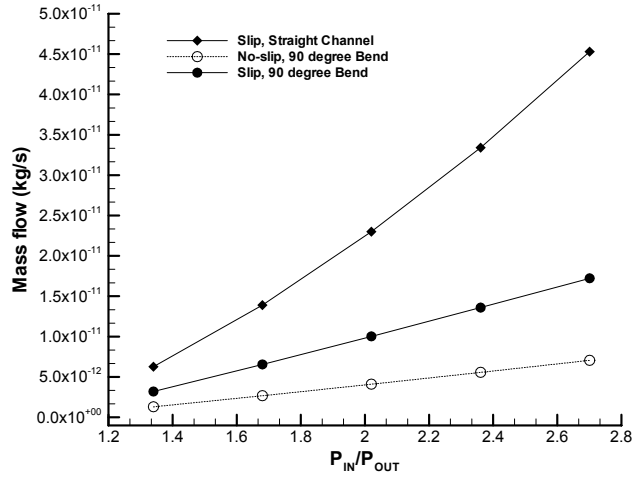

Fig 7: Numerical massflow comparison for the five pressure ratios for slip and no-slip flow for the micro-column with 90^o bends and corresponding massflow for a straight microchannel.

CONCLUSION

A finite element based hydrodynamic model has been developed to simulate gaseous flow through complex micro-geometries. The applicability of the algorithm has been extended to analyze low speed Nitrogen flow through a micro-column with two 90^o bends for an outlet Knudsen number of 0.0585. The gaseous flow has been modeled using both no-slip and first order slip boundary conditions. The results clearly capture the effect of slip on the walls showing a ~55% higher streaming velocity than the corresponding no-slip solution. Slip flows also show significantly higher massflow rates. The twisted geometry of the present study reduces the massflow rate by ~160% than that for a straight microchannel with the same overall dimensions. The analysis indicates suitability of the algorithm for efficiently predicting flows through practical microfluidic devices. The developed algorithm can also easily incorporate high order boundary conditions discussed in literature. Our future effort will address this issue to simulate gaseous flows with higher Knudsen number.

REFERENCES

[1] Beskok, A., Karniadakis, G.E. and Trimmer, W., 1996, "Rarefaction and Compressibility effects in Gas microflows", *Journal of Fluids Engineering* , **118** ,pp.448-456.

[2] Schaaf, S.A. and Chambre, P.L., 1961, *Flow of rarefied gases*, Princeton University Press, Princeton, New Jersey.

[3] Harley, J.C., Huang, Y. and Bau, H., 1995, "Gas flow in microchannels." *Journal of Fluid Mechanics,* **284**, pp. 257-74.

[4] Liu, J., Tai, Y. C., Pong, K. and Ho, C. M., 1993, "Micromachined channel/pressure sensor systems for micro flow studies", *The 7th International Conference on Solid-state Sensors and Actuators*, *Transducers'93,* pp.995-998.

[5] Liu, J., Tai, Y.C., and Ho, C.M., 1995, "MEMS for pressure distribution studies of Gaseous flows in microchannels", *Proceedings, IEEE Micro Electro Mechanical Systems Workshop, Amsterdam*, pp. 209-215.

[6] Chen, C.S., Lee, S.M. and Sheu J.D., 1998, "Numerical analysis of gas flow in microchannels." *Numerical Heat Transfer, Part A,* **33**, pp.749-62.

[7] Pong, K.C., Ho, C., Liu, J. and Tai, Y.C., 1994, "Non-linear pressure distribution in uniform microchannels." *Application of Microfabrication to Fluid Mechanics,* FED – **197**, pp.51-6.

[8] Arkilic, E.B., Schimidt, M.A. and Breuer, K.B., 1997, "Gaseous slip flow in long microchannels", *Journal of Microelectromechanical systems*, **6**(2), pp. 167-178.

[9] Arkilic, E.B., Breuer, K.S. and Schmidt, M.A., 1994, "Gaseous Flow in Microchannel", *Application of Microfabrication to Fluid Mechanics, ASME,* FED- 197, pp. 57-66.

[10] Karniadakis, G.E. and Beskok, A., 2002, *Micro Flows-Fundamentals and Simulation*, Springer-Verlag, New York.

[11] Beskok, A. and Karniadakis, G.E., 1992, "Simulation of Slip-flows in complex micro-geometries", *Micromechanical Systems***,** *ASME*, DSC-**40***,* pp. 355-370.

[12] Roy, S., Raju, R., Chuang, H., Kruden, B. and Meyyappan, M., 2003, "Modeling gas flow through microchannels and nanopores", *Journal of Applied Physics*, **93** (8), pp. 4869-4878.

[13] Maxwell, J.C., 1879, "On stresses in rarefied gases arising from inequalities of temperature." *Philosophical Transactions of the Royal Society Part 1,* **170**, pp. 231-56.

[14] Smoluchowski, von M., 1898, "Ueber wärmeleitung in verdünnten gasen." *Annalen der Physik und Chemi,* **64**, pp. 101-30.

[15] Arkilic, E.B., 1997, "Measurement of the Mass Flow and Tangential Momentum accommodation coefficient in silicon micromachined channels", Ph.D. Thesis, MIT, Massachusetts.

[16] Arkilic, E.B., Breuer, K.B. and Schimidt, M.A, 2001, "Mass flow and tangential momentum accommodation in silicon micromachined channels", *Journal of Fluid Mechanics*, **437**, pp. 29-43.

[17] Beskok, A. and Karniadakis, G.E., 1994, "Simulation of Heat and Momentum transfer in complex micro-geometries", AIAA J. Therm. & Heat Transfer, **8**(4), pp.647-655.

[18] Sreekanth, A.K., 1969, "Slip Flow through Long Circular Tubes", *Rarefied Gas Dynamics, eds. Trilling, L. and Wachman, H. Y., Academic Press, New York* **, 1**, pp. 667-680,

[19] Piekos, E. and Breuer, K., 1995, "DSMC modeling of microchannel devices", *AIAA Thermophysics Conference, San Diego*, *CA*, AIAA 95-2089.

[20] Oden, J.T. and Oliveira, E.R.A., 1976, *Lectures on Finite Element Methods in Continuum Mechanics*, The University of Alabama in Huntsville Press, Huntsville.

[21] Roy, S. and Baker, A.J., 1998, "A nonlinear subgrid embedded finite element basis for accurate monotone steady CFD solutions – Part II: Benchmark Navier-Stokes solutions," *Numerical Heat Transfer – Part B,* **33**(1), pp. 5-36.

[22] Roy, S. and Pandey, B.P., 2002, "Plasma-Wall Interaction inside a Hall Thruster." *Journal of Plasma Physics*, **68**(4), pp. 305-319.

[23] Roy, S. and Pandey, B.P., 2002, "Numerical Investigation of a Hall Thruster Plasma." *Physics of Plasma,* **9**(9), pp. 4052-2060.

[24] Balagangadhar, D. and Roy, S., 2001, "Design Sensitivity Analysis and Optimization of Steady Fluid-Thermal Systems", *Computer Methods in Appl. Mechanics and Engineering,* **190**(42), pp. 5465-5479.

[25] Roy, S., 2000, "Combining Galerkin matrix perturbation with Taylor weak statement algorithms", *Computer Methods in Appl. Mechanics and Engineering*, **184** (1-2), pp. 87-98.

[26] Baker, A.J., Iannelli, J., Chaffin D.J. and Roy, S., 1998, "Some recent adventures into improved finite element CFD methods for convective transport", *Computer Methods in Applied Mechanics and Engineering*, **151**, pp.27-42.

[27] Richtmyer, R.D. and Morton, K.W., 1967, *Difference Methods for Initial-Value Problems*, 2nd Ed, Interscience Publishers, Wiley, New York.